Biomedical Optics EXPRESS

Functional optical coherence tomography of rat olfactory bulb with periodic odor stimulation

Hideyuki Watanabe,[1,2] Uma Maheswari Rajagopalan,[3] Yu Nakamichi,[1] Kei M. Igarashi,[4] Hirofumi Kadono,[5] and Manabu Tanifuji[1,*]

[1]*Laboratory for Integrative Neural Systems, RIKEN Brain Science Institute, 2-1 Hirosawa, Wako-city, Saitama, 351-0198, Japan*
[2]*Course of Health Science, Graduate school of Medicine, Osaka University, 1-7 Yamada-oka, Suita, Osaka, 565-0871, Japan*
[3]*Department of Food Life Sciences, Faculty of Food Life Sciences, Toyo University, 1-1-1 Izumino, Itakura-machi, Ora-gun, Gunma, 374-0193, Japan*
[4]*Department of Anatomy and Neurobiology School of Medicine University of California, Irvine Hall Room 112, California 92697, USA*
[5]*Graduate School of Science and Engineering, Saitama University, 255 Shimo-Okubo, Sakura-ku, Saitama-city, Saitama, 338-08570, Japan*
[*]*tanifuji@riken.jp*

Abstract: In rodent olfactory bulb (OB), optical intrinsic signal imaging (OISI) is commonly used to investigate functional maps to odorant stimulations. However, in such studies, the spatial resolution in depth direction (z-axis) is lost because of the integration of light from different depths. To solve this problem, we propose functional optical coherence tomography (fOCT) with periodic stimulation and continuous recording. In fOCT experiments of in vivo rat OB, propionic acid and m-cresol were used as odor stimulus presentations. Such a periodic stimulation enabled us to detect the specific odor-responses from highly scattering brain tissue. Swept source OCT operating at a wavelength of 1334 nm and a frequency of 20 kHz, was employed with theoretical depth and lateral resolutions of 6.7 µm and 15.4 µm, respectively. We succeeded in visualizing 2D cross sectional fOCT map across the neural layer structure of OCT in vivo. The detected fOCT signals corresponded to a few glomeruli of the medial and lateral parts of dorsal OB. We also obtained 3D fOCT maps, which upon integration across z-axis agreed well with OISI results. We expect such an approach to open a window for investigating and possibly addressing toward inter/intra-layer connections at high resolutions in the future.

©2016 Optical Society of America

OCIS codes: (170.2655) Functional monitoring and imaging; (170.3880) Medical and biological imaging; (170.4500) Optical coherence tomography; (170.6900) Three-dimensional microscopy; (170.6935) Tissue characterization; (170.5380) Physiology; (070.2615) Frequency filtering; (170.3010) Image reconstruction techniques.

References and links

1. B. D. Rubin and L. C. Katz, "Optical imaging of odorant representations in the mammalian olfactory bulb," Neuron **23**(3), 499–511 (1999).
2. N. Uchida, Y. K. Takahashi, M. Tanifuji, and K. Mori, "Odor maps in the mammalian olfactory bulb: domain organization and odorant structural features," Nat. Neurosci. **3**(10), 1035–1043 (2000).
3. A. Grinvald, E. Lieke, R. D. Frostig, C. D. Gilbert, and T. N. Wiesel, "Functional architecture of cortex revealed by optical imaging of intrinsic signals," Nature **324**(6095), 361–364 (1986).
4. T. Bonhoeffer and A. Grinvald, "Optical Imaging Based on Intrinsic Signals," in *Brain Mapping The Methods,* A. W. Toga, J. C. Mazziotta eds. (Academic Press, 1996), pp. 55–97.
5. F. Pain, B. L'heureux, and H. Gurden, "Visualizing odor representation in the brain: a review of imaging techniques for the mapping of sensory activity in the olfactory glomeruli," Cell. Mol. Life Sci. **68**(16), 2689–2709 (2011).
6. M. Meister and T. Bonhoeffer, "Tuning and topography in an odor map on the rat olfactory bulb," J. Neurosci. **21**(4), 1351–1360 (2001).
7. L. Belluscio and L. C. Katz, "Symmetry, stereotypy, and topography of odorant representations in mouse olfactory bulbs," J. Neurosci. **21**(6), 2113–2122 (2001).

#256150 Received 21 Dec 2015; revised 7 Feb 2016; accepted 8 Feb 2016; published 10 Feb 2016

8. M. Luo and L. C. Katz, "Response correlation maps of neurons in the mammalian olfactory bulb," Neuron **32**(6), 1165–1179 (2001).
9. K. Mori, Y. K. Takahashi, K. M. Igarashi, and M. Yamaguchi, "Maps of odorant molecular features in the Mammalian olfactory bulb," Physiol. Rev. **86**(2), 409–433 (2006).
10. R. Vincis, O. Gschwend, K. Bhaukaurally, J. Beroud, and A. Carleton, "Dense representation of natural odorants in the mouse olfactory bulb," Nat. Neurosci. **15**(4), 537–539 (2012).
11. S. Sasaki, I. Yazawa, N. Miyakawa, H. Mochida, K. Shinomiya, K. Kamino, Y. Momose-Sato, and K. Sato, "Optical imaging of intrinsic signals induced by peripheral nerve stimulation in the in vivo rat spinal cord," Neuroimage **17**(3), 1240–1255 (2002).
12. I. Kida, F. Xu, R. G. Shulman, and F. Hyder, "Mapping at glomerular resolution: fMRI of rat olfactory bulb," Magn. Reson. Med. **48**(3), 570–576 (2002).
13. R. U. Maheswari, H. Takaoka, H. Kadono, R. Homma, and M. Tanifuji, "Novel functional imaging technique from brain surface with optical coherence tomography enabling visualization of depth resolved functional structure in vivo," J. Neurosci. Methods **124**(1), 83–92 (2003).
14. D. Huang, E. A. Swanson, C. P. Lin, J. S. Schuman, W. G. Stinson, W. Chang, M. R. Hee, T. Flotte, K. Gregory, C. A. Puliafito, and J. G. Fujimoto, "Optical coherence tomography," Science **254**(5035), 1178–1181 (1991).
15. M. Wojtkowski, "High-speed optical coherence tomography: basics and applications," Appl. Opt. **49**(16), D30–D61 (2010).
16. S. A. Boppart, B. E. Bouma, C. Pitris, J. F. Southern, M. E. Brezinski, and J. G. Fujimoto, "In vivo cellular optical coherence tomography imaging," Nat. Med. **4**(7), 861–865 (1998).
17. J. G. Fujimoto, "Optical coherence tomography for ultrahigh resolution in vivo imaging," Nat. Biotechnol. **21**(11), 1361–1367 (2003).
18. Y. Yasuno, V. D. Madjarova, S. Makita, M. Akiba, A. Morosawa, C. Chong, T. Sakai, K. P. Chan, M. Itoh, and T. Yatagai, "Three-dimensional and high-speed swept-source optical coherence tomography for in vivo investigation of human anterior eye segments," Opt. Express **13**(26), 10652–10664 (2005).
19. K. Tsunoda, K. Fujinami, and Y. Miyake, "Selective abnormality of cone outer segment tip line in acute zonal occult outer retinopathy as observed by spectral-domain optical coherence tomography," Arch. Ophthalmol. **129**(8), 1099–1101 (2011).
20. Y. Muraoka, H. O. Ikeda, N. Nakano, M. Hangai, Y. Toda, K. Okamoto-Furuta, H. Kohda, M. Kondo, H. Terasaki, A. Kakizuka, and N. Yoshimura, "Real-time imaging of rabbit retina with retinal degeneration by using spectral-domain optical coherence tomography," PLoS One **7**(4), e36135 (2012).
21. R. U. Maheswaria, H. Takaoka, R. Homma, H. Kadono, and M. Tanifuji, "Implementation of optical coherence tomography (OCT) in visualization of functional structures of cat visual cortex," Opt. Commun. **202**(1-3), 47–54 (2002).
22. U. M. Rajagopalan and M. Tanifuji, "Functional optical coherence tomography reveals localized layer-specific activations in cat primary visual cortex in vivo," Opt. Lett. **32**(17), 2614–2616 (2007).
23. A. D. Aguirre, Y. Chen, J. G. Fujimoto, L. Ruvinskaya, A. Devor, and D. A. Boas, "Depth-resolved imaging of functional activation in the rat cerebral cortex using optical coherence tomography," Opt. Lett. **31**(23), 3459–3461 (2006).
24. Y. Chen, A. D. Aguirre, L. Ruvinskaya, A. Devor, D. A. Boas, and J. G. Fujimoto, "Optical coherence tomography (OCT) reveals depth-resolved dynamics during functional brain activation," J. Neurosci. Methods **178**(1), 162–173 (2009).
25. V. J. Srinivasan, S. Sakadzić, I. Gorczynska, S. Ruvinskaya, W. Wu, J. G. Fujimoto, and D. A. Boas, "Depth-resolved microscopy of cortical hemodynamics with optical coherence tomography," Opt. Lett. **34**(20), 3086–3088 (2009).
26. A. D. Mehta, J. C. Jung, B. A. Flusberg, and M. J. Schnitzer, "Fiber optic in vivo imaging in the mammalian nervous system," Curr. Opin. Neurobiol. **14**(5), 617–628 (2004).
27. V. A. Kalatsky and M. P. Stryker, "New paradigm for optical imaging: temporally encoded maps of intrinsic signal," Neuron **38**(4), 529–545 (2003).
28. V. A. Kalatsky, D. B. Polley, M. M. Merzenich, C. E. Schreiner, and M. P. Stryker, "Fine functional organization of auditory cortex revealed by Fourier optical imaging," Proc. Natl. Acad. Sci. U.S.A. **102**(37), 13325–13330 (2005).
29. C. N. Guy, D. H. ffytche, A. Brovelli, and J. Chumillas, "fMRI and EEG responses to periodic visual stimulation," Neuroimage **10**(2), 125–148 (1999).
30. L. M. Parkes, P. Fries, C. M. Kerskens, and D. G. Norris, "Reduced BOLD response to periodic visual stimulation," Neuroimage **21**(1), 236–243 (2004).
31. P. Sun, J. L. Gardner, M. Costagli, K. Ueno, R. A. Waggoner, K. Tanaka, and K. Cheng, "Demonstration of tuning to stimulus orientation in the human visual cortex: a high-resolution fMRI study with a novel continuous and periodic stimulation paradigm," Cereb. Cortex **23**(7), 1618–1629 (2013).
32. S. A. Engel, G. H. Glover, and B. A. Wandell, "Retinotopic organization in human visual cortex and the spatial precision of functional MRI," Cereb. Cortex **7**(2), 181–192 (1997).
33. Y. Nakamichi, V. A. Kalatsky, H. Watanabe, U. M. Rajagopalan, and M. Tanifuji, "3D structure of the orientation column in cat primary cortex revealed by functional optical coherence tomography," Abstr. Soc. Neurosci. **270.01** (2011), *http://www.abstractsonline.com/Plan/ViewAbstract.aspx?sKey=d023089b-a64b-4aa9-b3cb-6129bde54e45&cKey=09b7566c-c153-4692-8113-1a04e1af0b1d&mKey=%7b8334BE29-8911-4991-8C31-32B32DD5E6C8%7d*
34. H. Watanabe, U. M. Rajagopalan, Y. Nakamichi, K. M. Igarashi, V. D. Madjarova, H. Kadono, and M. Tanifuji, "In vivo layer visualization of rat olfactory bulb by a swept source optical coherence tomography and its confirmation through electrocoagulation and anatomy," Biomed. Opt. Express **2**(8), 2279–2287 (2011).

#256150 Received 21 Dec 2015; revised 7 Feb 2016; accepted 8 Feb 2016; published 10 Feb 2016

35. H. Watanabe, U. M. Rajagopalan, Y. Nakamichi, K. M. Igarashi, H. Kadono, and M. Tanifuji, "Swept source optical coherence tomography as a tool for real time visualization and localization of electrodes used in electrophysiological studies of brain in vivo," Biomed. Opt. Express **2**(11), 3129–3134 (2011).
36. J. Binding, J. Ben Arous, J. F. Léger, S. Gigan, C. Boccara, and L. Bourdieu, "Brain refractive index measured in vivo with high-NA defocus-corrected full-field OCT and consequences for two-photon microscopy," Opt. Express **19**(6), 4833–4847 (2011).
37. Y. Watanabe, "Real time processing of Fourier domain optical coherence tomography with fixed-pattern noise removal by partial median subtraction using a graphics processing unit," J. Biomed. Opt. **17**(5), 050503 (2012).
38. D. H. Choi, H. Hiro-Oka, K. Shimizu, and K. Ohbayashi, "Spectral domain optical coherence tomography of multi-MHz A-scan rates at 1310 nm range and real-time 4D-display up to 41 volumes/second," Biomed. Opt. Express **3**(12), 3067–3086 (2012).

1. Introduction

In rodent olfactory bulb (OB), odor-evoked functional map has been commonly investigated by optical intrinsic signal imaging (OISI) [1,2]. OISI that has a lateral resolution of a few micrometers resolution does not need any exogenous treatment and can cover over large cortical areas [1–10]. However, in OISI due to imaging by a CCD system, the OISI map is visualized as integration of detected light from different depths and hence there is no spatial resolution for depth direction (z-axis). Therefore in OB, which consists of different neural layers, layer specific information is lost. Optical sectioning at different focus points with OISI was reported [11]. Even in such cases, it is difficult to increase z-axis spatial resolution to a few micrometers level. Apart from OISI, fMRI is a widely used functional brain imaging technique for obtaining functional map of OB [3,12]. However, fMRI does not support a few micrometers level of spatial resolution for both lateral and depth. As a way to overcome these difficulties, we propose the use of functional optical coherence tomography (fOCT) [13] for visualization of depth-resolved functional map of OB under high spatial resolutions.

Optical coherence tomography (OCT) [14–16] that forms the basis for the technology of fOCT. OCT visualizes depth-resolved biological structures as optical differences arising out of the spatial variations of the refractive index. OCT can provide high-resolutions of 1-15 μm [17]. OCT has already been employed as a diagnostic tool for imaging of retina in ophthalmology [18–20], and applied for various biological studies. In the initial stage, fOCT as a functional brain imaging was proposed to cat visual cortex. The fOCT signal was calculated from the recorded OCT time course data as changes of the OCT signal to visual stimulation [21,22]. fOCT was later demonstrated by different groups to rat somatosensory cortex under forepaw electrical stimulation [23–25].

However, one potential problem of fOCT is that the signal is weak, due to nature of highly scattering property of the brain tissue. The noise is sometimes expected to be larger than the fOCT signal as optical response [26]. In the case of OISI, a paradigm using periodic stimulation and continuous recording was demonstrated to discriminate stimulus specific optical responses, clearly [27,28]. The paradigm, by focusing on the periodic stimulus frequency, enables to minimize the effects of animal's physiological noise such as heartbeat and respiration in the signal [27]. Apart from optical imaging, functional MRI studies using such a paradigm were reported [29–32].

In fOCT also, as a way to achieve efficient response signal, we demonstrated stimulus specific signal to periodic visual stimulation from cat visual cortex at high resolution [33]. Based on these, in the current fOCT study, we employed a periodic simulation paradigm to obtain depth-resolved functional odor-evoked response maps of rat OB with high-resolution. As stimulus, we used two different odors, namely propionic acid and m-cresol. The stimuli are well known to evoke different dorsal area of OB by OISI [1,2,9]. Furthermore, our previous studies [34, 35] have already established OCT structural imaging of in vivo rat OB as a valid approach. Thus there is an advantage in conducting this study. In those studies, we reported cross sectional layered structure and its confirmation with anatomy. Our earlier studies showed that OCT enabled us to visualize different OB layers structure including glomerular layer (GL), external plexiform layer (EPL), mitral cell body layer (MCL) and granule cell layer (GCL) in vivo with a few micrometers of spatial resolution. Therefore, in this study, detected fOCT signal could be identified to the location of the corresponding structural layers at a few micrometer levels, precisely. Moreover, a comparison investigation of fOCT maps and OISI maps was performed for the same odorant stimuli.

#256150 Received 21 Dec 2015; revised 7 Feb 2016; accepted 8 Feb 2016; published 10 Feb 2016
(C) 2016 OSA

2. Methods

2.1 Animal preparation

Sprague-Dawley rats (SLC Japan, 5-7 weeks, 180-250 g) were anesthetized with medetomidine hydrochloride (Orion, Domitor, 0.5 mg/kg i.m.) and ketamine hydrochloride (Daiichi-Sankyo, Ketalar, 50-75 mg/kg i.p.). Four rats were used for writing this paper. The body temperature was maintained at 36.0-37.0 degrees Celsius with a temperature controlled heat blanket (Nihon Kohden, ATB-1100). The heartbeat was continuously monitored during the experiment by a heart rate counter equipped with a bioelectric amplifier (Nihon Kohden, AT-601G and AB-621G). The rats were mounted on a stereotaxic frame with an ear-bar set (NARISHIGE). Only the dorsal right OB was exposed after removing the skull with a dental drill. The surface of dorsal part was filled with mineral oil (Sigma, M3516), and covered with a round cover slip of diameter 22 mm (MATSUNAMI, C022001). During the experiments, we kept the heart rate of the animals to be around 250-320/min. Thiopental sodium (Mitsubishi Tanabe Pharma, Ravonal, 20 mg/kg/h i.p.) was injected in order to maintain a stable anesthetized condition. The experimental protocol was approved by the Animal Experiments Committee of RIKEN that follows the guideline of the National Institute of Health.

2.2 Experimental system of functional optical coherence tomography (fOCT)

The experimental system of fOCT consisted of an automated custom-made olfactometer (odorant stimulator) and a fiber based SS-OCT system (Fig. 1). Periodic odor stimulation was performed by the olfactometer. The odorant was diluted with mineral oil to 1:10 (Sigma, M3516), and 200 µl of the diluted odorant was loaded into the filter (Whatman, GD/X 25 Syringe Filter GF/D 2.7 µm, 6888-2527). The odorant molecules were carried to the output tube by pumping (Enomoto Micro Pump, GA-6EA) the charcoal filtered air. The total airflow of approximately 2000 ml/min was kept by flow meters (Kojima instrument, RK1250). The duration of stimulus presentation was controlled by solenoid valves (ASCO Japan, 458300632EP-J) using DIO board kit (National Instruments, PCI-DIO-32HS, ER-16) and software (National Instruments, Labview). The output tube from the olfactometer was placed approximately 1 mm in front of right nasal cavity of the rat. Constant and continuous airflow in the tube was kept during the whole recording.

The SS-OCT system used a swept laser source (Santec, HSL-2000) having a central wavelength of 1334 nm, a full width half maximum (FWHM) of 117 nm, and an average output power of 18.1 mW. The imaging depth in air was 2.9 mm. The theoretical values for depth and lateral resolutions were 6.7 µm and 15.4 µm, respectively. Scanning speed of the swept source laser was 20 kHz. The details of SS-OCT system were described in our previous study [34]. The recording software was customized using the OCT software library of Santec written in LabVIEW (National Instruments). When each OCT volume image was saved into HDD (Hitachi, HDS723020BLA642, 7200 rpm, 2TB), the SS-OCT system received also the presented stimulus ID (for example, no stimulus: 0, m-cresol: 1, propionic acid: 2) using UDP network protocol from the olfactometer, and the recording software added the presented stimulus ID to the corresponding OCT volume data.

#256150 Received 21 Dec 2015; revised 7 Feb 2016; accepted 8 Feb 2016; published 10 Feb 2016
(C) 2016 OSA

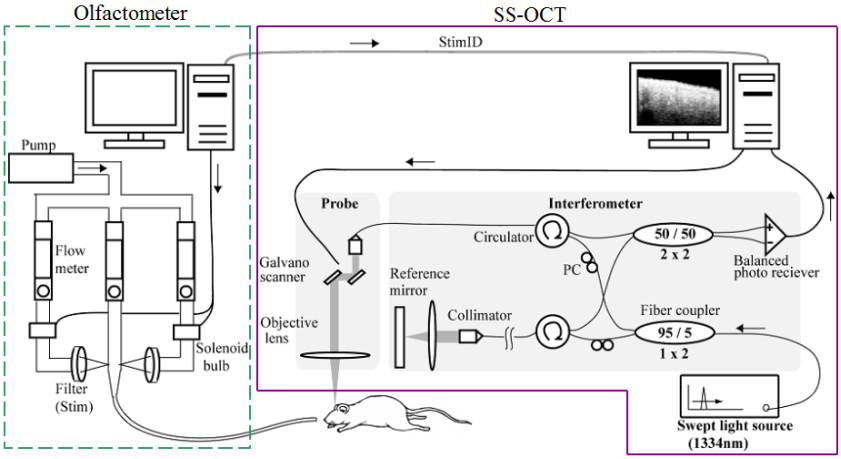

Fig. 1. A schematic view of the fOCT experimental system. The SS-OCT system is shown with magenta lines, and olfactometer is shown with green dash lines. The olfactometer sent odorant molecules to right nasal cavity of rat by air pump. Duration of stimulus presentation was controlled by solenoid valve. The airflow of stimulation was controlled by flow meters (left and right: 50-100 ml/min, center: 1900-2000 ml/min). The olfactometer sent stimulus ID to SS-OCT system using UDP network protocol. SS-OCT was operated at a wavelength of 1334 nm and a frequency of 20 kHz. The 1x2 fiber coupler with a coupling ratio 95/5 near the light source splits the light from the source respectively to sample arm (95%) and reference arm (5%). The 2x2 fiber coupler with a coupling ratio of 50/50 was used to combine reflected lights from the sample and the reference arms and this provides equally divided interference signal to be detected by the balanced receiver. OCT lateral scanning was performed by the galvano scanners. The OCT system had theoretical depth and lateral resolutions of 6.7 μm and 15.4 μm, respectively.

2.3 Periodic stimulus presentation paradigm

A paradigm showing a schematic temporal sequence of periodic stimulus presentation and the expected OCT component of the OCT signal to the stimulation were given in Fig. 2(a). As assumptions, OCT component was defined as expected stimulus evoked sinusoidal response that was completely synchronized to stimulus presentation cycle:1/60 Hz (0.0167 Hz). The odor stimuli, propionic acid (Wako Chem., 169-04723, CAS NO: 79-09-4) and m-cresol (Wako Chem., 169-04723, CAS NO: 108-39-4) were presented every 60 sec, continuously. The duration of each stimulus was set as 10 sec, and the stimulus presentation of m-cresol was shifted by 30 sec to the presentation of the other stimulus, propionic acid. Expected fOCT signal as optical response signals were indicated by colors violet and green, respectively. Here, components 1 and 2 were the expected sinusoidal modulations, synchronized to the stimulus frequency 0.0167 Hz. Especially, amplitude and phase at 0.0167 Hz correspond to signal intensity and stimulus selectivity, respectively. Propionic acid and m-cresol have been well investigated in OISI of OB [2,6–9]. OISI images to propionic acid in Fig. 2(c) and m-cresol in Fig. 2(d), along with a CCD image of imaging region in Fig. 2(b), were displayed. The regions indicated by red dotted lines in Fig. 2(b) and 2(e) showed a schematic view of the OCT scanning area.

#256150 Received 21 Dec 2015; revised 7 Feb 2016; accepted 8 Feb 2016; published 10 Feb 2016
(C) 2016 OSA

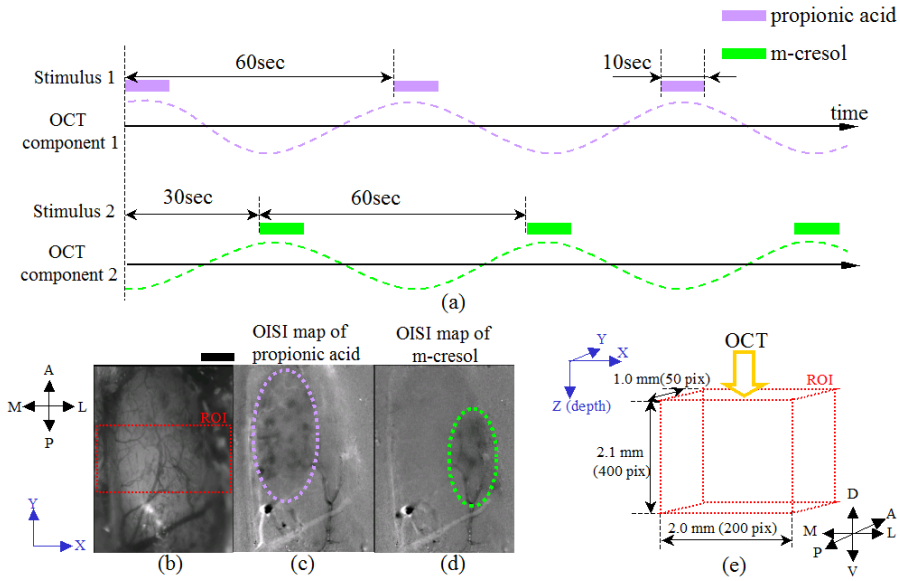

Fig. 2. (a) A schematic of the temporal sequence of periodic stimulus presentation of 0.0167 Hz and expected responses of sinusoidal OCT components to the frequency of 0.0167 Hz. M-cresol was presented with 30 seconds delay to propionic acid. Duration of stimulus presentation was set as 10 seconds. (b) CCD image of right OB to OISI samples (c, d). (c) OISI map to propionic acid. (d) OISI map to m-cresol. Odor-evoked optical responses of OISI were identified in magenta and green regions. Scale bar, 500 µm. (e) Schematic image indicates OCT scanning area (red dotted lines) with the scan parameters. A, anterior; P, posterior; L, lateral; M, medial; D, dorsal; V, ventral.

2.4 Data acquisition and processing of OCT

Continuous OCT recording was performed at a rate of 0.5 volumes/sec for around 4 hours (7000-7500 volumes) to periodic stimulus presentation. For getting A-scan data of OCT, λ-k (wavelength-wave number) conversion and FFT computation were performed with the recorded raw OCT data. One volume data of OCT corresponded to 400 pixels (z-axis) × 200 pixels (x-axis) × 50 pixels (y-axis) in Fig. 2(e), and it corresponded to 2.1 mm (2.9 mm in air) × 2.0 mm × 1.0 mm, respectively. The refractive index of the brain tissue was assumed to be 1.38 [36]. The voxel size corresponded to 5.25 µm (z-axis) × 10 µm (x-axis) × 20 µm (y-axis). All computations were done offline.

2.5 Calculation of fOCT signal

fOCT signal was calculated with common logarithmic scale by software (Mathworks, Matlab) and 3D visualization software (Maxnet, Avizo). Initially, to minimize time-dependent axial movement errors, 50 B-scan images (all zx-planes) were corrected individually for misalignment by calculation of 2D cross correlation. A diagram of the flowchart to obtain fOCT data was shown in Fig. 3.

(1) To obtain a complex OCT data at the stimulus frequency 0.0167 Hz, FFT computation (Length: 2^{13}) was performed with time course OCT 4D data.

(2) 3D Gaussian spatial filtering was applied to the complex OCT data at 0.0167Hz. The pixel size of the filter was set as 19 pixels (z-axis) × 10 pixels (x-axis) × 5 pixels (y-axis). The length of one side corresponds to 100 µm. The size of σ and FWHM were selected as 21.3 µm and 50µm (FWHM≈2.35 × σ).

(3-a) Phase angle was calculated from the spatial filtered complex OCT data.

(3-b) Magnitude data was calculated from the spatial filtered complex OCT data. Magnitude data (0 to 1) was calculated from square of normalized amplitude (0 to 1).

#256150 Received 21 Dec 2015; revised 7 Feb 2016; accepted 8 Feb 2016; published 10 Feb 2016
(C) 2016 OSA

(4-a) The phase angle can take a value in the range of 0 to 2π. To distinguish stimulus dependency of fOCT signal, the phase angle was mapped by 8-bit pseudo-color image of RGB HSV color space (cylindrical coordinate).

(4-b) fOCT signal intensity was described by the magnitude.

Specifically, the magnitude of fOCT signal was expressed by using alpha channel of TIFF format. The alpha channel enables us to control the transparency of target color. The degree of intensity of colors shows intensity of fOCT signal. Phase data of (4-a) was used as the target color. As background, black image or cross sectional OCT image were used. Integrated fOCT maps across depth (Fig. 8) were obtained by matrix summation to "fOCT data (3D)" of Fig. 3 for z-axis (depth).

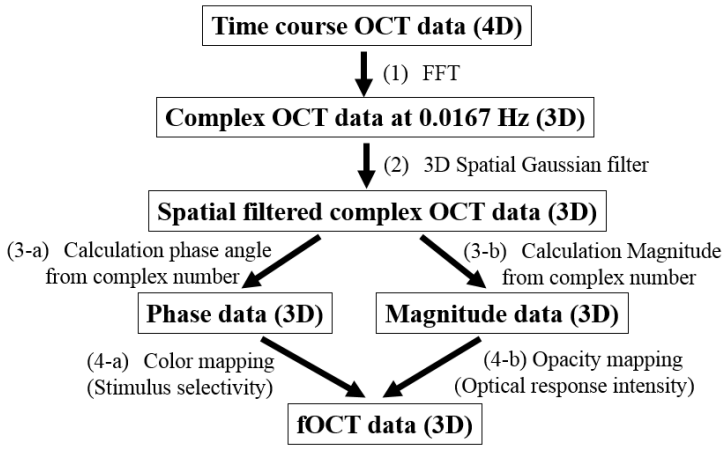

Fig. 3. Flowchart to obtain fOCT data.

2.6 Conventional optical intrinsic signal imaging (OISI)

We performed conventional OISI with block type stimulus presentation as a separate session of fOCT recording [4]. Same set of stimuli, propionic acid and m-cresol were presented by the olfactometer. The system of OISI consisted of a CCD monochrome video camera (CS8310, TELI) with tandem-lens arrangement (C-mount type 35 mm and 105 mm lenses (Nikon)) and a halogen lamp with appropriate wavelength filter attached. Prior to starting intrinsic signal recording, blood vessel patterns were captured by CCD at a wavelength of 539 nm. The intrinsic signal recording was done at a wavelength of 692 nm. The video signal was captured and digitized by a 10-bit PCI frame grabber (Pulsar, Matrox). The acquired image data were processed by the custom-made acquisition software that resized the image size to 320 × 240 pixels after 2 × 2 spatial binning. The temporal resolution was 2 Hz after the temporal binning. ROI of OISI covered 2.8 mm × 2.1 mm ranges of dorsal right OB. For each stimulus, OISI recording was performed for 15 trials, and OISI map was visualized by trial averaging. One trial corresponded to 8 sec, with 2 sec before stimulation, and 6 sec during stimulation. Inter trial interval was set to be approximately 30 sec.

3. Results and Discussion

3.1 Cross sectional fOCT maps under stimulus and control conditions

Figure 4(a) shows a CCD image of the OB surface of rat #0. Corresponding 3D OCT image was integrated across the z-axis (depth) to give a surface image as shown in Fig. 4(b). The surface vessel pattern agreed well with the CCD image of OB surface. Green arrows in Fig. 4(a)-4(c) indicated the blood vessel from the same location of the OB surface. Figure 4(c) and 4(d) show the cross sectional OCT image and the respective fOCT image obtained with two different stimuli. These images corresponded to the blue dotted lines on the surface image in Fig. 4(a) and Fig. 4(b). In deriving the fOCT image, the normalized amplitude image and the phase image were used (Fig. 4(e) and Fig. 4(f)). Here normalization was done using the square amplitude of the complex data. In Fig.

#256150 Received 21 Dec 2015; revised 7 Feb 2016; accepted 8 Feb 2016; published 10 Feb 2016
(C) 2016 OSA

4(d), we found two circular spots indicated by white arrows, shown in green and magenta. These circular spots of Fig. 4(d) matched to the strong signals pointed by red arrow in amplitude map (Fig. 4(e)). The phase difference corresponded to the difference in timing of stimulus presentations (30 sec). Spatially, the magenta spot in the medial part of OB and the green spot in the lateral part of OB were observed. The relative spatial positions of these spots agreed with the OISI data (Fig. 2(c), 2(d)). This result was also consistent with the existing reports of OISI maps with the medial part of OB activated by propionic acid while m-cresol activated the lateral dorsal region [5,9]. In order to confirm the validity of the functional signal, as a control experiment, OCT scans were performed without odor stimulation at the same position across the blue line of Figs. 4(a), and 4(b). Cross sectional OCT image and fOCT image under control experiment were shown in Fig. 4(g) and Fig. 4(h), respectively. For comparison, the normalized amplitude image (Fig. 4(i)) and phase image (Fig. 4(j)) were also given at the frequency of 0.0167 Hz. Two regions as indicated by the white arrows in Fig. 4(h) corresponded to the supposed spots of Fig. 4(d). As seen, the spots were absent. The absence of specific spots under null stimulation showed that fOCT in conjunction with periodic stimulation paradigms is capable of giving stimulus specific signals.

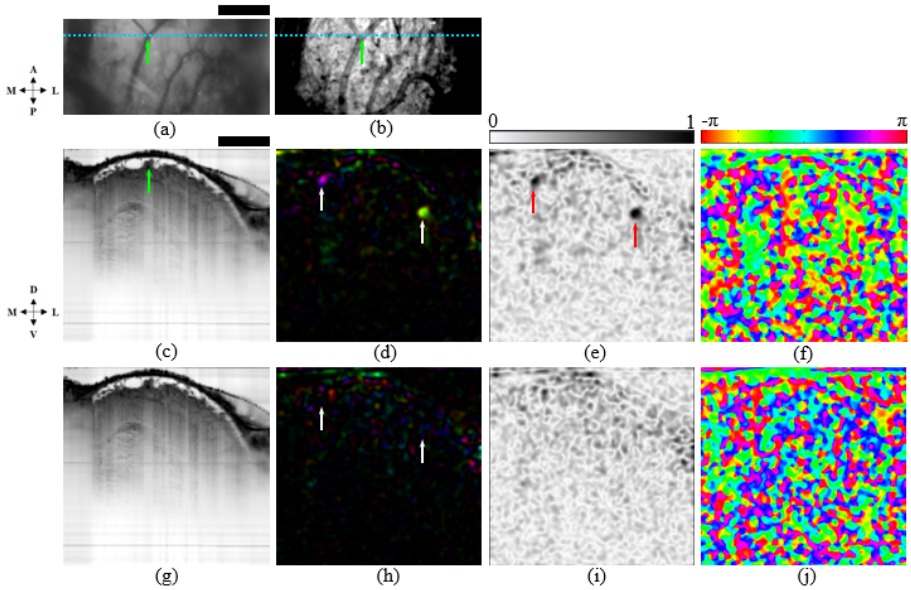

Fig. 4. (a) CCD image of OB surface. (b) Integrated OCT image across z-axis obtained at the same position of (a). (c) Cross sectional OCT image corresponded to blue dot line of (a) and (b), at periodic odor stimulus condition. Green arrows in 4(a-c) indicated the same blood vessel. (d) fOCT map having magnitude and phase information to periodic odor stimulation. Amplitude map (e) and phase map (f) to periodic odor stimulation. (g) Cross sectional OCT image corresponded to blue dot line of (a) and (b), under control experiment (no stimulus condition). (h) fOCT image under control experiment. Amplitude map (i) and phase map (j) under control experiment. Two spots indicated by the white arrows were detected functional signals in (d) and (h). The red arrows showed same position of the white arrows. A, anterior; P, posterior; L, lateral; M, medial; D, dorsal; V, ventral. Scale bar, 500 μm.

3.2 fOCT signal from neural layer structure of OB

Next, we investigated the spatial correspondence between the detected fOCT signal and in vivo OB neural layer structure (rat #1). Again for the sake of comparison, the surface image obtained with a CCD camera and the one obtained from integrating 3D OCT image were shown in Fig. 5(a) and Fig. 5(b), respectively. The blue dotted lines in either figure indicated the corresponding cross sectional OCT image (Fig. 5(c)) and the fOCT image (Fig. 5(d)). The region indicated by white squares in Fig. 5(c) and Fig. 5(d) were magnified and shown in Fig. 5(e) with corresponding fOCT image in Fig. 5(f). The white arrows in Fig. 5(f) were identified to be the fOCT signals from the blood vessels

#256150 Received 21 Dec 2015; revised 7 Feb 2016; accepted 8 Feb 2016; published 10 Feb 2016
(C) 2016 OSA

indicated by white arrows in Fig. 5(e). The magnified cross sectional OCT image (Fig. 5(e)) showed neural layer structures: GL, EPL, MCL, and GCL. The detected in vivo anatomical neural layer structure by SS-OCT matched well to our previous reports [34,35]. Further, a few glomeruli were observed at GL in Fig. 5(e). For clarification, we showed the same images in Fig. 5(g) and 5(h) with a few glomeruli encircled in red dotted lines. As can be seen clearly from Fig. 5(h), the magenta and green spots nearly confine to a few encircled circular regions of glomeruli. The overlaid image (Fig. 5(i)) was reconstructed from the cross sectional OCT image of Fig. 5(c) and the fOCT image of Fig. 5(d). The image of Fig. 5(i) demonstrated that fOCT recording enabled us to visualize functional signals and the corresponding cross sectional neural layer structure of OB at micrometer resolution level, simultaneously.

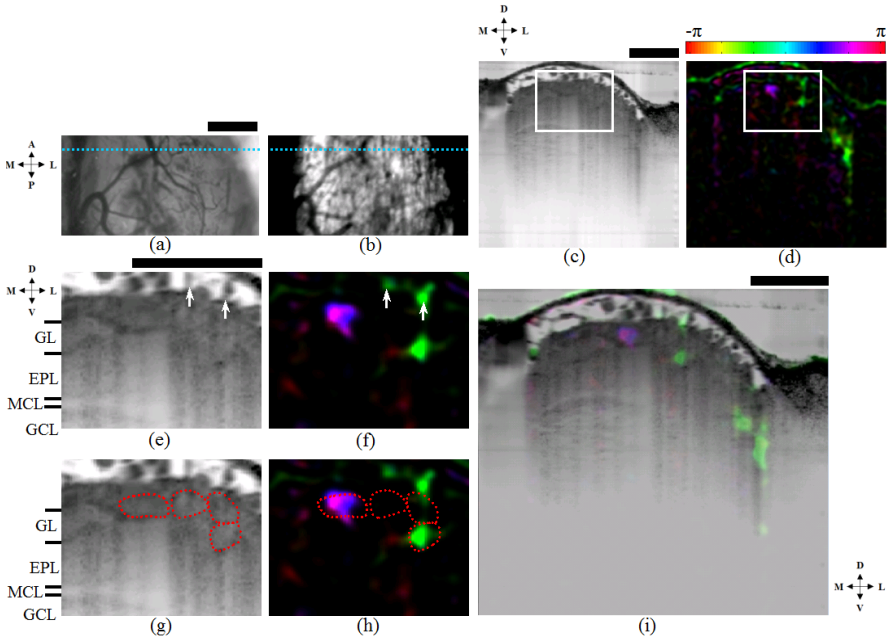

Fig. 5. (a) CCD image of OB surface. (b) Integrated OCT image in z-axis. (c) Cross sectional OCT image corresponded to the blue dotted line of (a) and (b). (d) fOCT image to the periodic odor stimulation to the blue dot line of (a) and (b). (e) Magnified OCT image to white square of (c). (f) Magnified fOCT image to white square of (d). (g) Same OCT image to (e) and a few glomeruli were encircled by red dotted line. (h) Same fOCT image to (f) and a few glomeruli were encircled by red dotted line. (i) Overlaid image of using OCT image of (c) and fOCT image of (d). A, anterior; P, posterior; L, lateral; M, medial; D, dorsal; V, ventral. Scale bar, 500 μm.

Figure 6 showed the results of another OB, rat #2. The images were visualized by the same processing used for obtaining results of Fig. 5. The blue dotted lines of CCD image (Fig. 6(a)) and integrated OCT image (Fig. 6(b)) indicated the position of cross sectional OCT image (Fig. 6(c)) and fOCT image (Fig. 6(d)). Regions indicated by white squares in Fig. 6(c) and Fig. 6(d) were magnified and shown in Fig. 6(e) and Fig. 6(f), respectively. fOCT signal was detected at the white arrow in Fig. 6(f). It corresponded to the vessel indicated by the white arrow of Fig. 6(e). Again, in the same OCT and fOCT images were shown with a few glomeruli encircled in red dotted lines in Fig. 6(g) and 6(h). We identified responses clearly in Fig. 6(h) at some of the encircled specific glomeruli. Figure 6(i) was obtained by the overlaying the functional image of Fig. 6(d) onto the OCT image of Fig. 6(c). Figure 6(i) also demonstrated that the fOCT was capable of clearly localizing the responses from the neural layer structure in vivo for both odor stimuli, propionic acid and m-cresol.

#256150 Received 21 Dec 2015; revised 7 Feb 2016; accepted 8 Feb 2016; published 10 Feb 2016
(C) 2016 OSA

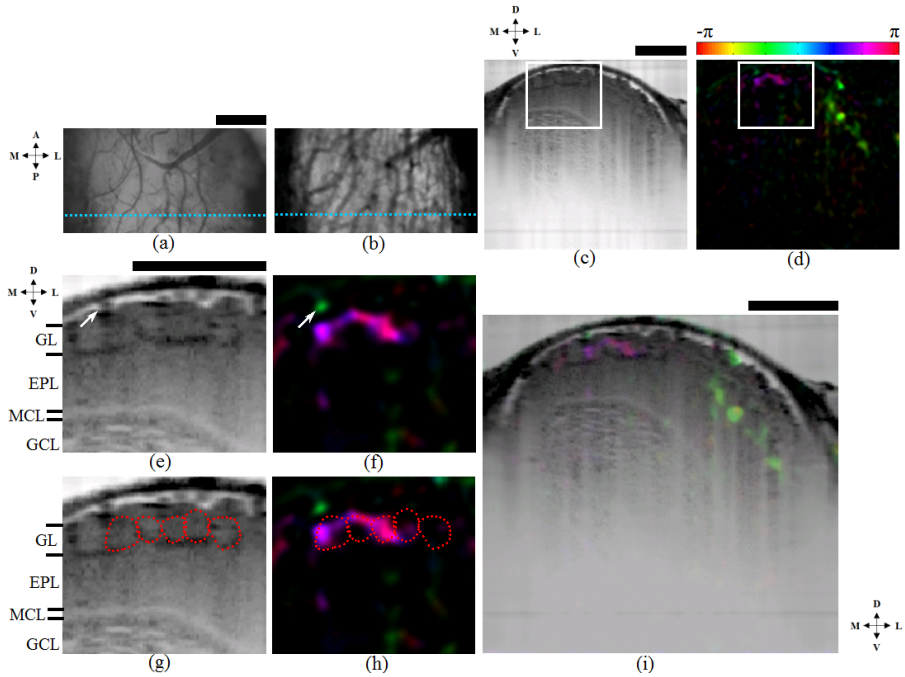

Fig. 6. (a) CCD image of OB surface. (b) Integrated OCT image in z-axis. (c) Cross sectional OCT image corresponded to the blue dotted line of (a) and (b). (d) fOCT image to the periodic odor stimulation to the blue dot line of (a) and (b). (e) Magnified OCT image to white square of (c). (f) Magnified fOCT image to white square of (c). fOCT signal was also detected at the vessel by the white arrow. (g) Same OCT image of (e) and a few glomeruli were encircled by red dotted line. (h) Same fOCT image of (f) and a few glomeruli were encircled by red dotted line. (i) Overlaid image of using OCT image of (c) and fOCT image of (d). A, anterior; P, posterior; L, lateral; M, medial; D, dorsal; V, ventral. Scale bar, 500 μm.

3.3 Visualization of 3D fOCT map to periodic stimulus presentation

3D fOCT maps in Fig. 7(a) and Fig. 7(e) were visualized from two different rat OBs corresponded to rat #1 and rat #2. The 3D fOCT images were reconstructed from 2D fOCT maps. Figures 7(b)-7(d) and Figs. 7(f)-7(h) were different views of the 3D image of Fig. 7(a) and Fig. 7(e), respectively. The distribution of 3D fOCT signal in Figs. 7(a)-7(d) was observed clearly as two groups of response signals. The response signal in the medial part of OB shown as magenta corresponded to propionic acid, the response signal at lateral part of OB as green corresponded to m-cresol. Then, the functional signals in 3D fOCT (Figs. 7(e)-7(h)) were also observed as two distinct, different distributions to the periodic stimulation of propionic acid and m-cresol as well as Fig. 7(a)-7(d).

#256150 Received 21 Dec 2015; revised 7 Feb 2016; accepted 8 Feb 2016; published 10 Feb 2016
(C) 2016 OSA

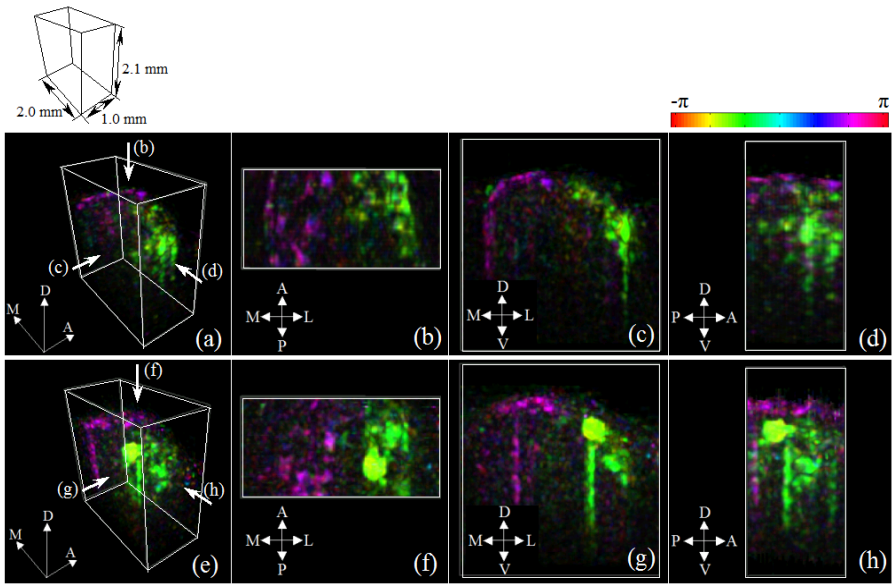

Fig. 7. (a) 3D fOCT image of OB (rat # 1). (b-d) Different views of 3D fOCT image (a) indicated by each white arrow in (a). (e) 3D fOCT image of another OB (rat # 2). (f-h) Different views of 3D fOCT image (e) indicated by each white arrow in (e). A, anterior; P, posterior; L, lateral; M, medial; D, dorsal; V, ventral.

3.4 Spatial relationship between fOCT map and conventional OISI map

A comparison of the 3D fOCT map was done with the intrinsic signal map. In order to make the comparison, at first 3D fOCT data was integrated across depth and the integration process was also done for OCT data to give a surface image. Integrated OCT image and integrated fOCT map in z-axis were shown in Fig. 8(a) and Fig. 8(b), to the same region of OB (rat #2). To the region, CCD image and OISI map were also shown in Fig. 8(c) and Fig. 8(d). In order to compare fOCT map and OISI map, the images were precisely aligned using the surface blood vessels of Fig. 8(a) and Fig. 8(c). As a result, fOCT map (Fig. 8(b)) and OISI map (Fig. 8(d)) were matched well, spatially. We identified that the encircled fOCT signals by white arrows in Fig. 8(b) corresponded to encircled OISI signals by white arrows in Fig. 8(d). Then, the correlation coefficients between the fOCT map and the OISI map to propionic acid and m-cresol were 0.694 and 0.739, respectively. In another rat (rat #1), Figs. 8(e-h) were obtained in the same way to Figs. 8(a-d). Spatial correspondence between fOCT map (Fig. 8(f)) and OISI map (Fig. 8(h)) were observed, for both over the fully imaged region, and also across the local regions encircled and indicated by white arrows. Specifically, in Fig. 8(f), right encircled fOCT signal corresponding to the response of m-cresol was detected to be better spatially resolved than the corresponding spot in the OISI map shown in Fig. 8(h). The correlation coefficients between the fOCT map and the OISI map to propionic acid and m-cresol were 0.637 and 0.620, respectively.

#256150 Received 21 Dec 2015; revised 7 Feb 2016; accepted 8 Feb 2016; published 10 Feb 2016
(C) 2016 OSA

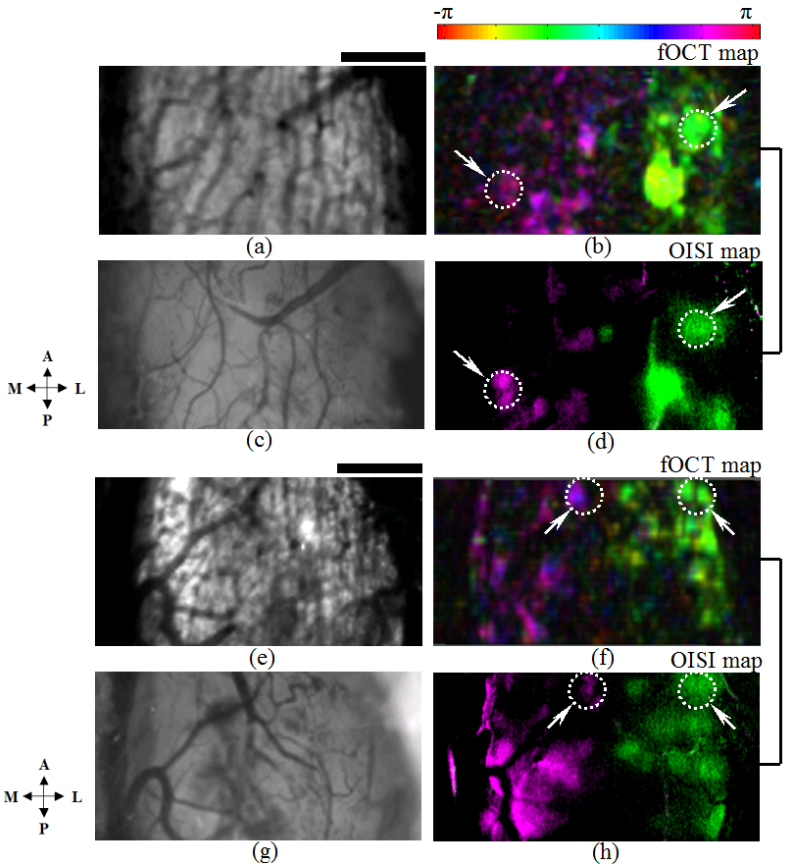

Fig. 8. Spatial relationship between fOCT map and conventional OISI map obtained from 2 OBs, with (a-d) of rat # 2, and (e-h) of rat # 1. (a, e) Integrated surface OCT images in z-axis. (b, f) Integrated fOCT images of (a, e). (c, g) CCD images of OB surface. (d, h) OISI maps of (c, g) with pseudo colors (green: m-cresol and magenta: propionic acid). The encircled local regions of fOCT maps pointed by white arrow could have better spatial resolution than the same regions of OISI maps. A, anterior; P, posterior; L, lateral; M, medial. Scale bar, 500 μm.

3.5 Temporal fOCT signal to stimulus presentation

In order to investigate the temporal synchronization to all signals (stimulation, the fOCT signal using paradigm with 1/60 Hz sine wave, and the time course OCT signal), we showed the results in Fig. 9. ROIs were selected from the center of fOCT spots indicated by arrows in magenta and green in Fig. 9(a) for rat #0. The ROI size was set as 100 μm (z-axis) × 100 μm (x-axis) × 100 μm (y-axis). First, to obtain the time courses fOCT signal within the ROIs, spatial/temporal averaging were performed for every 5 cycles (300 sec: 60 sec × 5 cycles), and normalized (−1 to 0). Figure 9(b) showed the calculated temporal fOCT signal as black line to stimulation of propionic acid. The duration time of presented stimulation was shown in light magenta bars (10 sec). Red dotted line was the calculated fOCT signal using paradigm. The periodic variation of the fOCT signal was synchronized to the stimulation of propionic acid. Figure 9(c) showed the temporal fOCT signal (black line) to stimulation of m-cresol (light green bars) and the fOCT signal using paradigm (green dot line). Again, we identified that the temporal fOCT signal to m-cresol synchronized with the periodic stimulation of m-cresol. In Fig. 9(d) and Fig. 9(e), one cycle variations (60 sec) of the temporal fOCT of Fig. 9(b) and Fig. 9(c) were shown. The temporal fOCT signal in Fig. 9(d) dropped down from the beginning of stimulation to the end of stimulation, and the signal gradually recovered back during no stimulus period. A similar tendency was identified in 9(e) where the signal dropped down from the

#256150 Received 21 Dec 2015; revised 7 Feb 2016; accepted 8 Feb 2016; published 10 Feb 2016
(C) 2016 OSA

beginning of stimulation to the end of stimulation, and the signal gradually recovered back during no stimulus period.

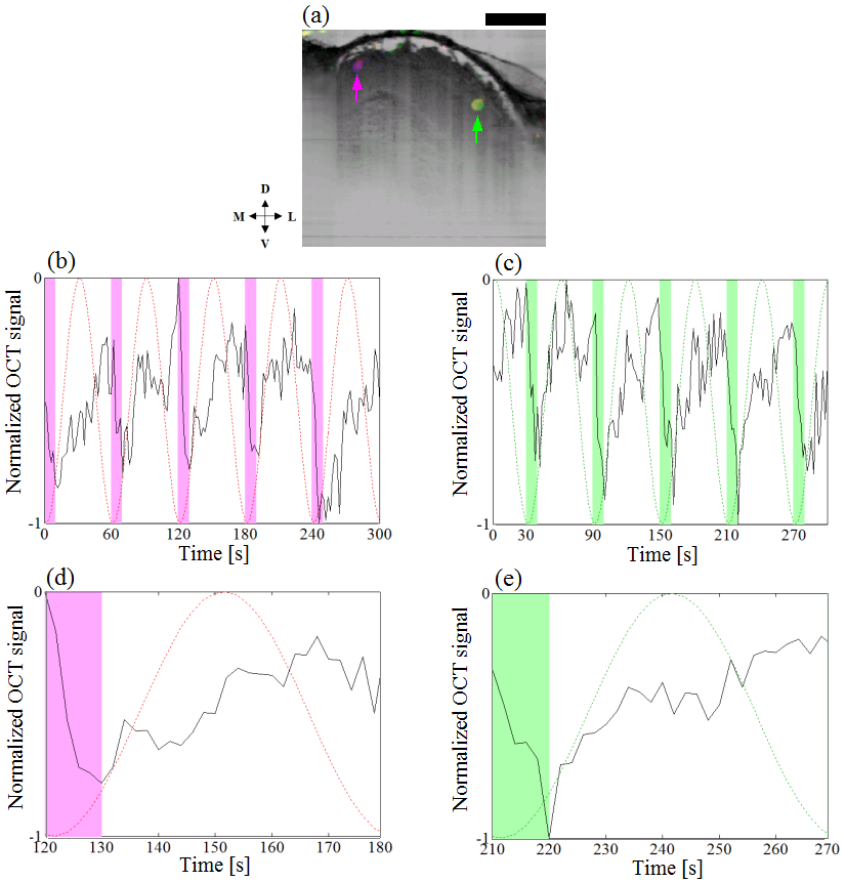

Fig. 9. (a) Cross sectional fOCT image obtained with periodic stimulation (rat #0). (b-e) Temporal fOCT signal (black line) and stimulus presentation period (each color bar indicates 10 sec) and dotted lines (detected periodic fOCT signal) were displayed. (b) Temporal fOCT signal to propionic acid. The target fOCT signal was pointed by the magenta color arrow in (a). (c) Temporal fOCT signal to m-cresol. The target fOCT signal was pointed by the green color arrow in (a). (d) and (e) were magnified one cycle images of (b) and (e) at a certain trial of one period of 60 sec. L, lateral; M, medial; D, dorsal; V, ventral. Scale bar, 500 μm.

4. Summary

Commonly, OISI has been used for investigation of functional map in rodent OB because OISI have advantages of lateral resolution and does not need any exogenous treatment. However, as a disadvantage, OISI map has no spatial resolution in depth direction. To solve this problem, we proposed using fOCT to investigate functional map of rodent OB. Further, to enhance the weak fOCT signal from high-scattering brain tissue, a paradigm using the periodic stimulation and continuous recording was proposed and demonstrated. In this study, we succeeded in visualizing depth-resolved fOCT map of rat OB. Moreover, this approach combined with our previous work that visualized rat OB neural layer structure by OCT, the combined method enabled us to compare functional map and neural layer structure, precisely, in micrometer level. It was a powerful neuro imaging technique for investigating functional map of rodent OB. For further details, in GL of OB, fOCT spots were localized to each glomerulus. By visualizing 3D fOCT map of rat OB, two distinctive distributions of stimulus-depended fOCT signal were clearly observed. From the results of fOCT map and conventional OISI map comparison, the relation of two maps showed a high positive correlation. Further, analysis of the temporal

#256150 Received 21 Dec 2015; revised 7 Feb 2016; accepted 8 Feb 2016; published 10 Feb 2016
(C) 2016 OSA

profile of detected fOCT signal showed synchronization between stimulation and fOCT signal using paradigm and temporal fOCT signal. One disadvantage of our current fOCT system is that the recording took about 4-4.5 hours at a rate of 0.5 volumes/sec because of the limitation from the speed of PC data transfer (memory). We thought there is a possibility to increase system speed by introducing high-speed memory and parallel signal computing technologies such as GPU or FPGA to the current system [36, 37]. At this stage, fOCT signal in GL was detected. In the future, we expect that this approach can be extended to detect functional signals from deeper neural layers such as EPL, MCL and GCL of rat OB, and such an approach promoting the investigation of inter/intra-layer connections at high resolutions.

Acknowledgments

We would like to thank Dr. Valery A. Kalatsky gave us the suggestion of applying periodic stimulation paradigm to our fOCT experimental system at early stage. We also thank Dr. Takayuki Sato, Dr. Kazunori O'hashi and Dr. Go Uchida for their advices on performing OISI experiment and signal processing. We thank the staff members of Research Resources Center in taking care of the animals. This work is supported by Grant-in-AID for Scientific Research 22300137, 26240021 and Grant-in-Aid for Scientific Research on Innovative Areas, “Sparse Modeling”, (25120004), JSPS, Japan. This work is also supported by the “Funding Program for World-leading Innovative R&D on Science and Technology (FIRST Program)”.